Heliyon 7 (2021) e06600

Contents lists available at ScienceDirect

Heliyon

journal homepage: www.cell.com/heliyon

Research article

Magnetite nanoparticles grafted with murexide-terminated polyamidoamine dendrimers for removal of lead (II) from aqueous solution: synthesis, characterization, adsorption and antimicrobial activity studies

Selma Ekinci [a,*], Zülfiye İlter [b], Selami Ercan [c], Ercan Çınar [c], Reşit Çakmak [d]

[a] Department of Chemistry, Faculty of Science and Art, Batman University, Batman, 72100, Turkey
[b] Department of Chemistry, Faculty of Science, Fırat University, Elazığ, 23000, Turkey
[c] Department of Nursing, School of Health Sciences, Batman University, Batman, 72060, Turkey
[d] Medical Laboratory Techniques Program, Vocational School of Health Services, Batman University, Batman, 72060, Turkey

ARTICLE INFO

Keywords:
Nanoparticles
Polyamidoamine dendrimers
Murexide
Adsorption
Antimicrobial activity

ABSTRACT

In this study, new, efficient, eco-friendly and magnetically separable nanoadsorbents, MNPs-G1-Mu and MNPs-G2-Mu, were successfully prepared by covalently grafting murexide-terminated polyamidoamine dendrimers on 3-aminopropyl functionalized silica-coated magnetite nanoparticles, and used for rapid removal of lead (II) from aqueous medium. After each adsorption process, the supernatant was successfully acquired from reaction mixture by the magnetic separation, and then analyzed by employing ICP-OES. Chemical and physical characterizations of new nanomaterials were confirmed by XRD, FT-IR, SEM, TEM, and VSM. Maximum adsorption capacities (q_m) of both prepared new nanostructured adsorbents were compared with each other and also with some other adsorbents. The kinetic data were appraised by using pseudo-first-order and pseudo-second-order kinetic models. Adsorption isotherms were found to be suitable with both Langmuir and Freundlich isotherm linear equations. The maximum adsorption capacities for MNPs-G1-Mu and MNPs-G2-Mu were calculated as 208.33 mg g^{-1} and 232.56 mg g^{-1}, respectively. Antimicrobial activities of nanoparticles were also examined against various microorganisms by using microdilution method. It was determined that MNPs-G1-Mu, MNPs-G2-Mu and lead (II) adsorbed MNPs-G2-Mu showed good antimicrobial activity against S. aureus *ATTC 29213 and C. Parapsilosis ATTC 22019*. MNPs-G1-Mu also showed antimicrobial activity against C. albicans *ATTC 10231*.

1. Introduction

Water pollution has been considered one of the most important environmental problems in the world. It has been already known that toxic and hazardous materials such as heavy metals and organic pollutants cause water pollution and deterioration of water quality. As a result of this case, water pollution has become a major health problem for human beings and other living things recently [1, 2, 3, 4, 5]. The reason is that heavy metals in water are toxic, and they lead to various diseases when they bioaccumulate in human body through the food chain. Lead is also one of these harmful heavy metals. It has an appearance of a slightly bluish, bright silvery metal in a dry atmosphere; and generally bioaccumulated in the bone; however it may influence any organ system. The effects of lead poisoning change depending on the amount of exposure and the age of the individual. Lead poisoning is excreted in feces and urine from human body, but it may also become visible in nails, hair, breast milk, and saliva [6, 7, 8, 9, 10]. Due to the toxic efficacies of lead on human body, it should be taken out from industrial wastewater [11].

A great deal of effort has been made to effectively and quickly isolate heavy metal ions from wastewater until now. For this purpose, the various conventional methods are commonly applied nowadays. One of the most common methods used for heavy metal removal is the adsorption process. This process has attracted great interest in that it is simple, economic and efficient [12, 13, 14, 15, 16, 17, 18].

One of the most important application areas of nanotechnology is wastewater. In recent years, scientists have been trying to produce new materials such as magnetic nanoparticles (MNPs) to use in the treatment of wastewater by nanotechnology. As a result of these studies, it has been determined that many modified novel nano-sized MNPs have been produced in the development and fabrication studies of alternative

* Corresponding author.
E-mail address: selma.ekinci@batman.edu.tr (S. Ekinci).

https://doi.org/10.1016/j.heliyon.2021.e06600
Received 14 October 2020; Received in revised form 18 December 2020; Accepted 23 March 2021

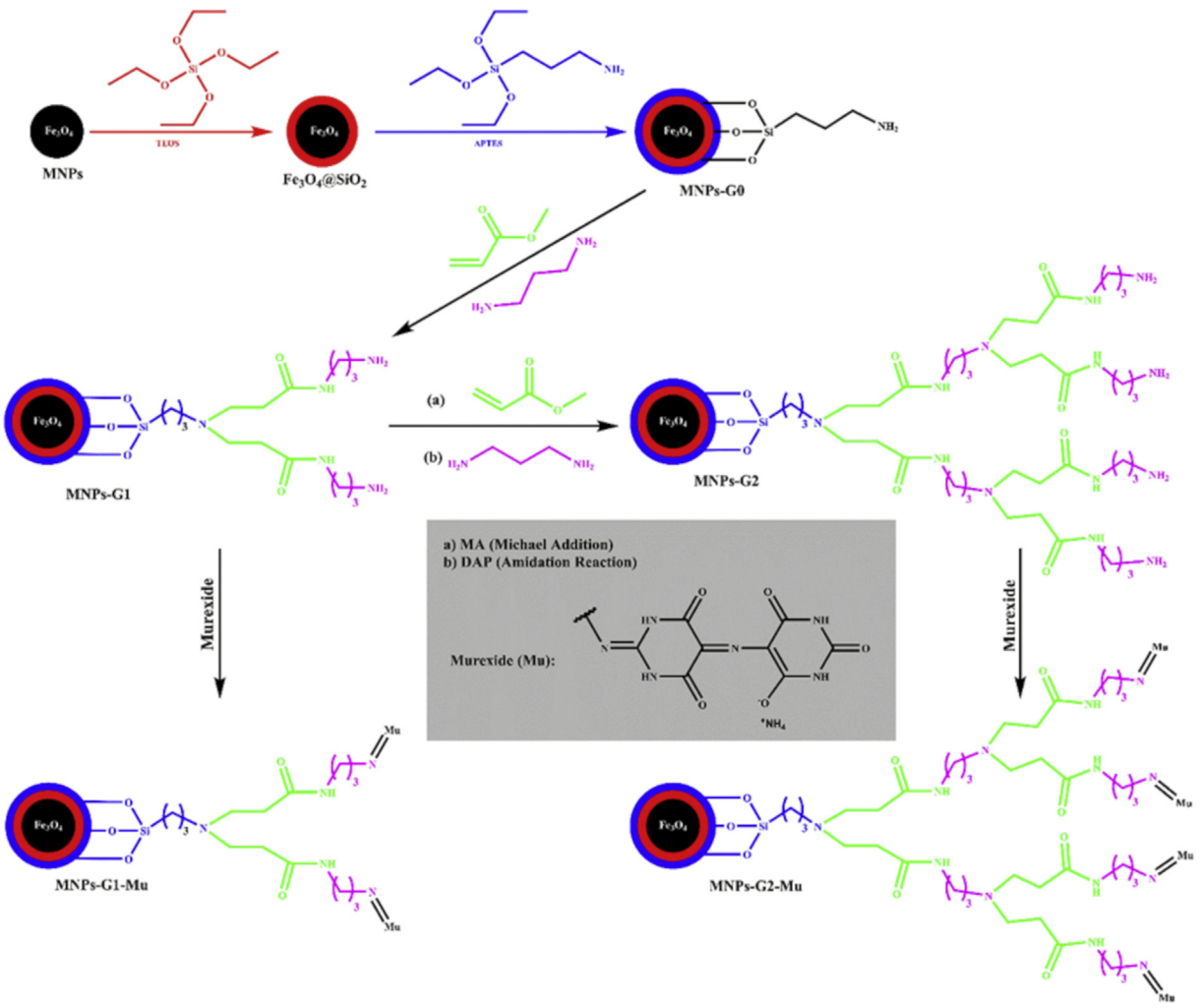

Figure 1. The schematic representation for the preparation of nanoadsorbents.

environmentally friendly and low-cost materials until now. MNPs, which have unique physical and chemical properties according to other particles, have been attracted great attention in the environment applications over the last years [19, 20, 21]. These nanoparticles are easily recovered from aqueous environment with the help of an external magnetic field without additional processes such as filtration or centrifugation because of their strong magnetic properties [22, 23, 24, 25]. However, such nanoparticles have tendency to oxidize in the air due to their high chemical activity. As a result of the oxidation reaction, their magnetic property and dispersity are reduced. For this reason, it is extremely important to improve some effective protection strategies for the coating of their surfaces with suitable materials (e.g. silica, polymer) and for the maintenance of their stability [26,27].

Dendrimers are hyperbranched polymers that have uniform structure. These polymers consist of core, branching units and branched functional groups. The variety of dendrimers is ensured by functional groups in their molecular structure. The branching units provide a continuous growth of the dendrimers. The degree of polymerization of the dendrimers is exhibited by the generation number (G), which represents the number of repetition cycles [28, 29, 30, 31].

Polyamidoamine dendrimers, namely PAMAM dendrimers, constitute one special class of dendritic polymers, which are one of the most important research topics at the present time. These macromolecules, with a wide ranges of potential applications such as chemical sensors, medical diagnostics, drug-delivery systems and the others, are considered as a kind of hyperbranched structures. In many studies, it was reported that these macromolecules were the first dendrimers, to be successfully prepared by using dendrimers synthesis methodology, characterized by different spectroscopic techniques, and then commercialized. They are frequently obtained by the repetition of two-step reactions. In the first step, methyl acrylate (MA) is added to amine groups on its molecular structure via Michael addition, and then in the second step, ethylenediamine or propylenediamine is grafted onto methyl ester groups by amidation reaction [32, 33, 34, 35].

PAMAM dendrimers have been used as a ligand for removal of hazardous materials such as heavy metal ions or dyes from wastewater or aqueous solutions in chemistry. It is known that the functional groups on their scaffold considerably increase the uptake capacity of heavy metal ions via coordination, ion exchange and chelation linkages (Figure 1). In some of the studies, it was reported that there is a surprising relationship between their adsorption capacity and increasing generations of PAMAM. While it is expected that higher generation dendrimers may show better adsorption efficiency owing to higher density of binding locations, their efficiency was conversely determined to decrease as the steric hindrance takes place at high generation of dendrimers [28, 36, 37, 38]. Therefore, 1st and 2nd generation dendrimers were used instead of 3rd generation dendrimers in the preparation of nanostructured adsorbents in this study.

Murexide (Mu), 5,5′-nitrilodibarbituric acid monoammonium salt or ammonium purpurate is slightly soluble in water and has the appearance of a reddish purple powder (Figure 1). It is commonly used in conventional ethylenediaminetetraacetic acid titrations. In addition to its

ordinary application as a metallochromic indicator, it has been utilized as an effective scavenger for hydroxyl and radicals superoxide, and lately as a chromogenic agent for traditional spectrophotometric determination of some metals [39, 40, 41, 42, 43]. For the preparation of new nano adsorbent, Mu is used as the metal ion binding agent because carbonyl groups in its molecular structure provide a great deal of advantage for conducting modification reactions and nitrogen atoms in its molecule can react with metal ions [40,44].

In recent years, more efficient, eco-friendly and magnetically separable novel adsorbents are still in urgent demand for more effective and rapid removal of heavy metal ions from wastewater, although many studies have reported on the preparation and use of PAMAM dendrimers or murexide functionalized magnetic nanoparticles, and magnetic separation has been also proposed an effective method for removal of heavy metals. As far as we know, there are no reports on the prepared iron oxide magnetite nanoparticles grafted with murexide-terminated polyamidoamine dendrimers as effective lead (II) adsorbent with antimicrobial activity. Unlike other similar nanostructured adsorbents in the current study, Mu was used as a metal binding agent by bonding to the end of polyamidoamine dendrimers for the first time by us.

The purpose of this study is to produce and characterize novel nanostructured adsorbents, which are characterized by many branched dendritic tree, by using Mu as lead (II) binding agent, and modified MNPs doped with PAMAM as carrier, and investigate their adsorption capacity for removing lead (II) from diluted solution, and also explore the antimicrobial activities of modified nanoparticles against different microorganisms by using microdillution method. All prepared nanomaterials were characterized by using X-Ray Diffraction (XRD), Fourier Transform Infrared Spectroscopy (FTIR), Scanning Electron Microscopy (SEM), Transmission Electron Microscopy (TEM), and Vibrating Sample Magnetometry (VSM), respectively. Inductively coupled plasma optical emission spectrometry (ICP-OES) was used for determination of lead (II) remaining in the samples after each adsorption process. Optimum adsorption conditions were determined by using batch method. Kinetics and isotherms studies of the adsorption of Pb (II) onto PAMAM dendrimers were carried out in detail. The maximum adsorption capacities of the used adsorbents for removal of lead (II) were compared with other reported adsorbents.

2. Materials and methods

2.1. Materials

All the chemicals purchased for the preparation of nanoadsorbents in the present study, iron (II) chloride tetrahydrate ($FeCI_2.4H_2O$), (Sigma-Aldrich); iron III) chloride hexahydrate ($FeCI_3.6H_2O$), (Sigma-Aldrich); concentrated ammonium hydroxide solution (NH_4OH), (Merck); tetraethylortosilicate ($Si(OC_2H_5)_4$), (Sigma-Aldrich); 3-aminopropyltriethoxysilane ($C_9H_{23}NO_3Si$), (Sigma-Aldrich); methyl acrylate ($C_5H_8O_2$), (Sigma-Aldrich); 1,3-diaminopropane ($NH_2(CH_2)_3NH_2$), (Merck); and murexide ($C_8H_8N_6O_6$), (Sigma-Aldrich), were utilized as received without any further purification. All the other chemicals were of analytical grade, and commercially available.

2.2. Analysis and characterization

In order to prepare the nanoadsorbents, a magnetic stirrer (Heidolph MR Hei-standart magnetic stirrer), a mechanical mixer (IKA Labortechnik RW 20), a sonication apparatus (Sonics), a cooled incubator (Zhicheng ZHWY-200 B incubator), a freeze dryer (Telstar LyoQuest), an oven (Memmert), and a pH meter (Hanna Instrument HI 221) were used. The characterization processes of nanoparticles were made by FT-IR (Thermo Scientific Nicolet iS5 FT-IR, wavenumber range of 400–4000 cm^{-1}), XRD (Bruker D8 advance high resolution diffractometer, filter K-beta (x1), scan range 10 000–80 000°, scan axis 2 Theta/Theta), SEM (Zeiss EVO MA 10, ADD dedector, acceleration voltage 15 kV, elevation degree 35, magnification 10 000 X), TEM (FEI Tecnai G2 spirit BioTwin, 120 kV) and VSM (Cryogenic limited PPMS). All aqueous solutions prepared in the current study were obtained by using deionized water (Mini pure water). Adsorption experiments were performed by using an orbital shaker (JP Selecta UR 6032011). The concentrations of lead (II) in the samples were measured by ICP-OES Spectrophotometer (Agilent 725 ICP-OES).

2.3. Preparation of MNPs-G0 as a starting material

MNPs-G0 was prepared in three steps by using the methods of modification reported previously [45,46].

The first step is the preparation of MNPs. Magnetic iron oxide nanoparticles were prepared according to methods reported by Çakmak et al., and Maity and Agrawal [47,48]. The second step is the preparation of silica-coated MNPs: silica coated MNPs (Fe_3O_4@SiO_2) were obtained by following the procedure of referenced articles and they were stored at +4 °C for further use [45,46].

The third step is the modification with APTES of silica-coated MNPs: 0.5 g of Fe_3O_4@SiO_2, dispersed in 50 mL of absolute ethanol, was sonicated for 1 h. After the sonication process, 4.2 g of APTES was added to the flask under continuous mechanical stirring, and the reaction was let to proceed at room temperature for 20 h under continuous mechanical stirring. Afterwards, the resultant products (MNPs-G0) were separated using an external magnetic field, and washed seven times with deionized water (100 mL) and ethanol (100 mL) and then dried at 70 °C (7 h) (Figure 1) and stored at +4 °C for later use [27].

2.4. Preparation of MNPs-G1-Mu and MNPs-G2-Mu

These absorbents were prepared in two and three steps by using MNPs-G0 as a starting nanomaterial.

The preparation of the first nano adsorbent (MNPs-G1-Mu): MA and DAP were firstly grafted on MNPs-G0 through Michael addition and amidation reaction, and then the resultant product (MNPs-G1) was reacted with Mu by a condensation reaction. Briefly, 2.0 g of MNPs-G0 was added in 100 mL of methanol and sonicated for 30 min to obtain the final dispersed suspension. Next, 20 mL of MA was added dropwise into the reaction medium while stirring the dispersed suspension vigorously for 30 min. Subsequently, the flask was sealed and the reaction was let to proceed at room temperature for 8 h under continuous mechanical stirring. The resultant material was rinsed with methanol for 5 times. Afterwards, they were mixed with 8 mL of DAP in 40 mL of methanol and stirred by using a mechanical stirrer for 3 h. After stirring, the resultant products (MNPs-G1) were separated using an external magnetic field, washed with methanol for 5 times [49]. Next, 10 g of dry MNPs-G1 and 10 g of Mu were dispersed in 100 mL of dimethyl sulfoxide (DMSO), and then the reaction mixture was refluxed at 120 °C for 24 h. The product (MNPs-G1-Mu) was separated by an external magnetic field, washed with DMSO and water until the filtrate displayed no color of Mu. In the end of these processes, the product was washed with methanol for three times, and then dried at 80 °C for 7 h [40].

The preparation of the second nano adsorbent (MNPs-G2-Mu): MA and DAP were firstly grafted on MNPs-G1, and then the resultant product (MNPs-G2) was reacted with Mu by a condensation reaction in DMSO to obtain the final product (MNPs-G2-Mu); and it was put out from the reaction medium by a magnet, rinsed with DMSO and water until the black color of Mu disappeared in the filtrate (Figure 1).

2.5. Experiments of adsorption

1000 mg L^{-1} stock solution of lead (II) was prepared by using $Pb(NO_3)_2$ and the stock solution was diluted at different concentrations to be used in adsorption experiments. The effects of equilibrium contact time (0–120 min), amount of adsorbent (0.125, 0.25, 0.5, 0.75 and 1.0 g), pH value (2, 3, 4, 4.5 and 5), and the initial concentration of Pb (II)

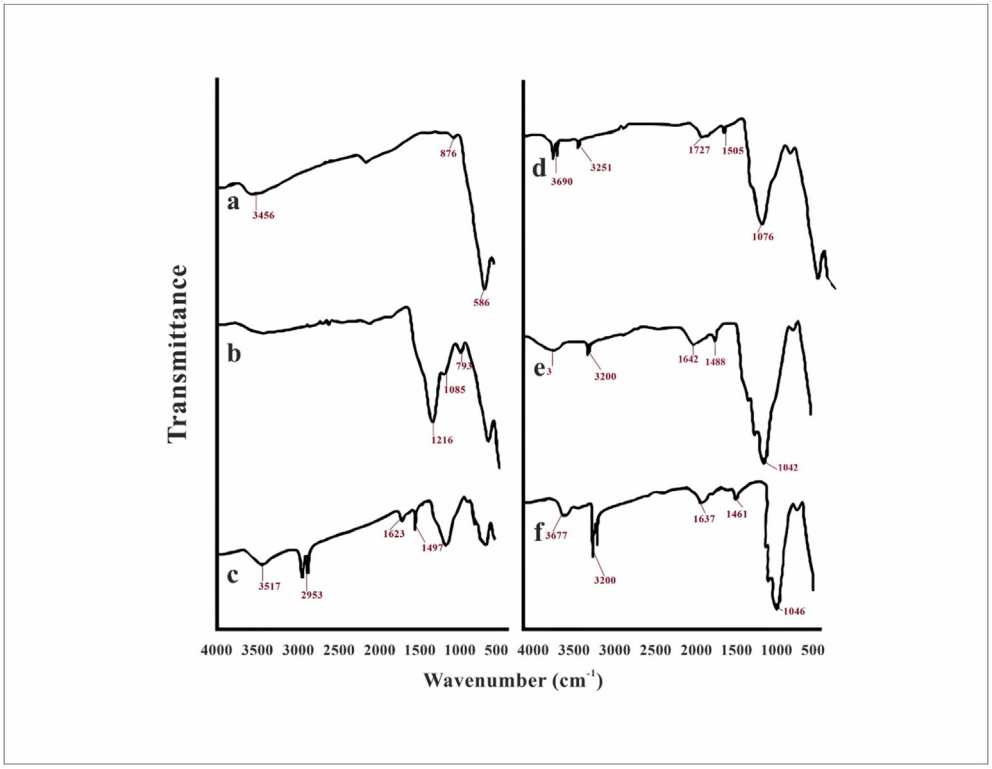

Figure 2. FT-IR spectra of a) MNPs, b) Fe_3O_4@SiO_2, c) MNPs-G0, d) MNPs-G1, e) MNPs-G1-Mu and f) MNPs-G2-Mu.

(25–200 mg L^{-1}) on the adsorption were investigated. 50 mg of adsorbents in 200 mL of 100 mg L^{-1} lead (II) solutions were mixed and shaken at 200 rpm for 120 min to determine the equilibrium contact time of the adsorptions. The other experiments of adsorption were carried out with 50 mL of lead (II) solutions and 50 mg of nanoadsorbents for 30 min. The pH values of lead (II) solutions were adjusted with 0,1 M of HCI and NaOH. After each shaking, the remaining amount of lead (II) in solutions was evaluated by using ICP-OES spectrophotometer. q_e (the adsorbed quantity of metallic ions) and A% (the adsorption percentage) were calculated from Eqs. (1) and (2):

$$q_e = \frac{(C_0 - C_e)xV}{m} \quad (1)$$

$$A\% = \frac{(C_0 - C_e)}{C_0} \times 100 \quad (2)$$

where C_o (mg L^{-1}) is the initial and C_e (mg L^{-1}) is the equilibrium concentration of heavy metal ions. V (L) is the volume of the solution and m is the mass of the adsorbent (g).

2.6. Investigation of antimicrobial activities

Due to the resistance developed by bacteria against antibiotics, the discovery or synthesis of new compounds with antimicrobial activity has become necessary. The substance that we synthesize and apply may open a horizon in reducing the microbial effect of bacteria that are resistant in this field. Therefore, antimicrobial activities of synthesized nanoparticles were investigated against *Staphylococcus Aureus ATTC 29213, Escherichia Coli ATCC 25922, Proteus Mirabilis ATTC 14153, Klebsiella Pneumoniae ATTC 4352, Enterococcus Faecalis ATTC 29212, Staphylococcus Aureus ATTC 29213, Pseudomonas Aeruginosa ATTC 27853, Candida Albicans ATTC 10231* and *Candida Parapsilosis* ATTC 22019 microorganisms by microdilution method [50, 51, 52, 53]. According to this method, antimicrobial agent was diluted in a series of liquid or solid medium. An equal amount of the microorganisms suspension was added to each dilution medium. The experimental series were incubated at the appropriate temperature (35–37 °C) and at the appropriate time for microbial growth (18–24 h). The lowest concentration (in μg mL^{-1}) of a substance that inhibits the growth of microorganisms is considered as Minimal Inhibition Concentration (MIC).

3. Results and discussion

3.1. Characterization

FT-IR, XRD, SEM, TEM and VSM techniques were used to characterize the structure and morphology of the synthesized nanoparticles.

3.1.1. FT-IR analysis

The surface modification of MNPs was characterized by FT-IR. As shown in Figure 2, in spectrum (a), vibrational stretching modes belong to Fe–O in 586 cm^{-1} and 876 cm^{-1} show that magnetic nanoparticles are formed [23,54, 55, 56, 57]. Broad band at 3456 cm^{-1} occurs because of the O–H strain vibration peak caused by adsorbed water and silanol groups in hydrogen-bonded [58, 59]. (b) It is understood from the peaks of Si–O–Si bond at 793 cm^{-1} and Si–O–Fe bond at 1085 cm^{-1} that silica is bound to MNPs [26]. The band at 1216 cm^{-1} belongs to the O–H vibration of adsorbed water [23,60]. (c) Peaks of N–H stretching vibration and free NH_2 groups were observed at 3517 and 1623 cm^{-1} respectively. The presence of the anchored alkyl group was confirmed by C–H stretching vibration at 2953 cm^{-1} [57,61]. The peak seen at 1497 cm^{-1} attached to the CH_2 group which has stretching vibration on aminopropyl groups, came into view at 2953 cm^{-1}. These peaks have also proved that the molecules of APTES bond to the iron oxide nanoparticles [62,63]. (d) The peak of vibration of the hydroxyl groups in C–O alcohol and Si–O bond was observed at 1076 cm^{-1} [54]. The stretching vibration of C=O associated with the steric group was seen in the band at 1727 cm^{-1} which proves the formation of PAMAM dendrimer [60,64]. The peak of the N–H groups associated with the first generation of PAMAM dendrimer (G1) was observed at 1505 cm^{-1} [65]. In spectrum (e) and (f) of the first and

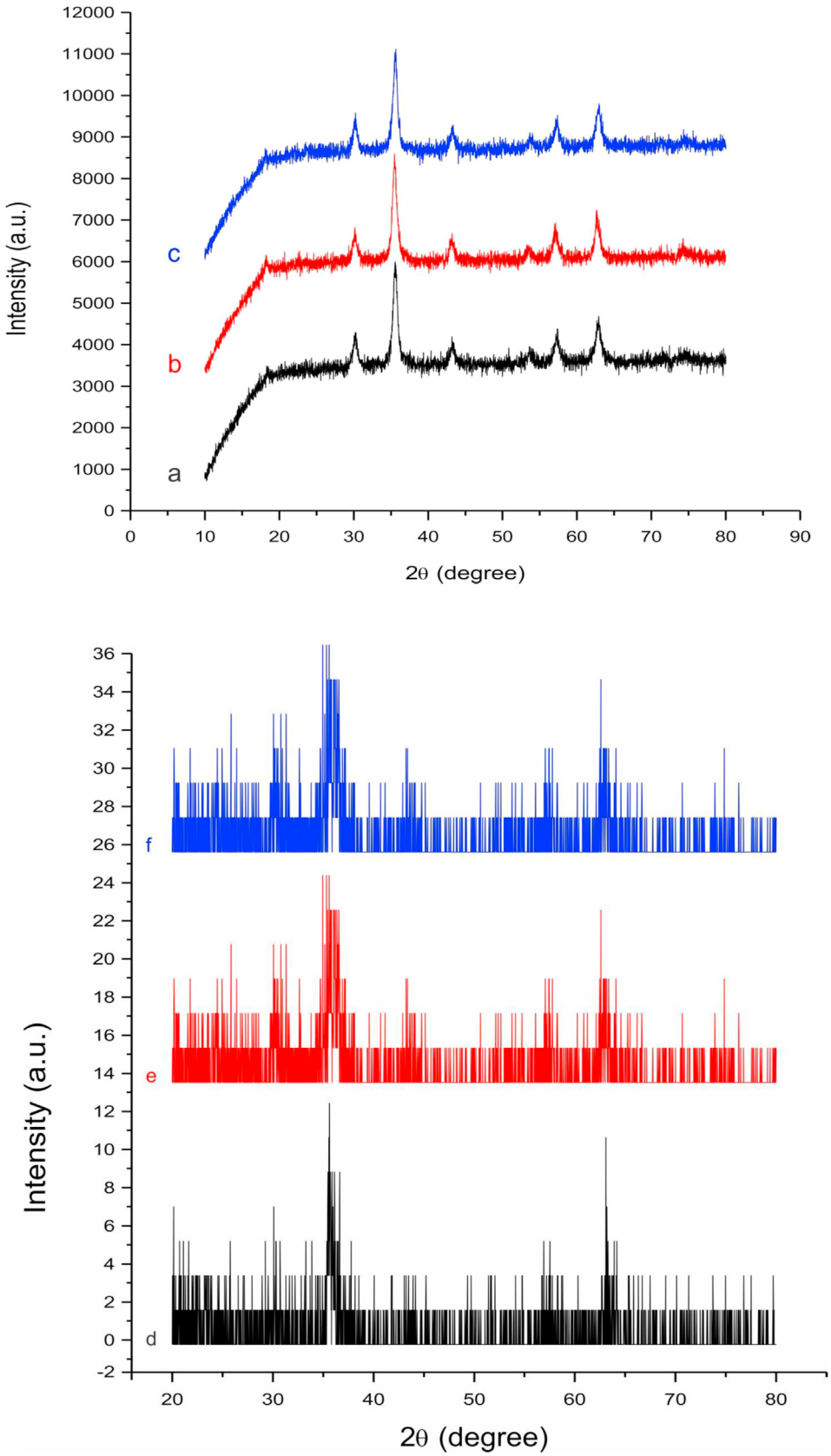

Figure 3. XRD graphics of a) MNPs, b) Fe_3O_4@SiO_2, c) MNPs-G0, d) MNPs-G1, e) MNPs-G1-Mu and f) MNPs-G2-Mu.

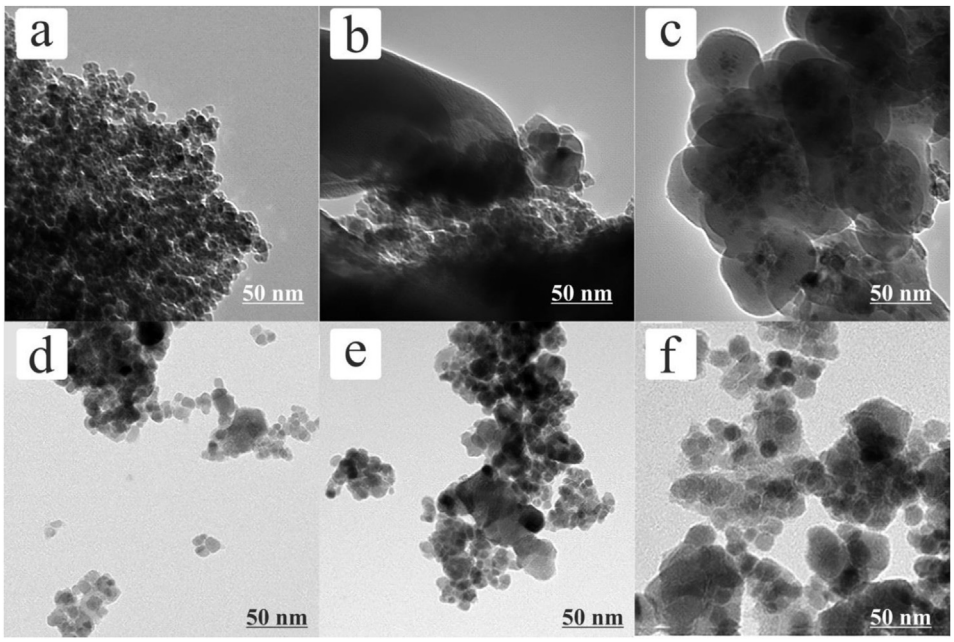

Figure 4. TEM images of a) MNPs, b) Fe_3O_4@SiO_2, c) MNPs-G0, d) MNPs-G1, e) MNPs-G1-Mu, f) MNPs-G2-Mu.

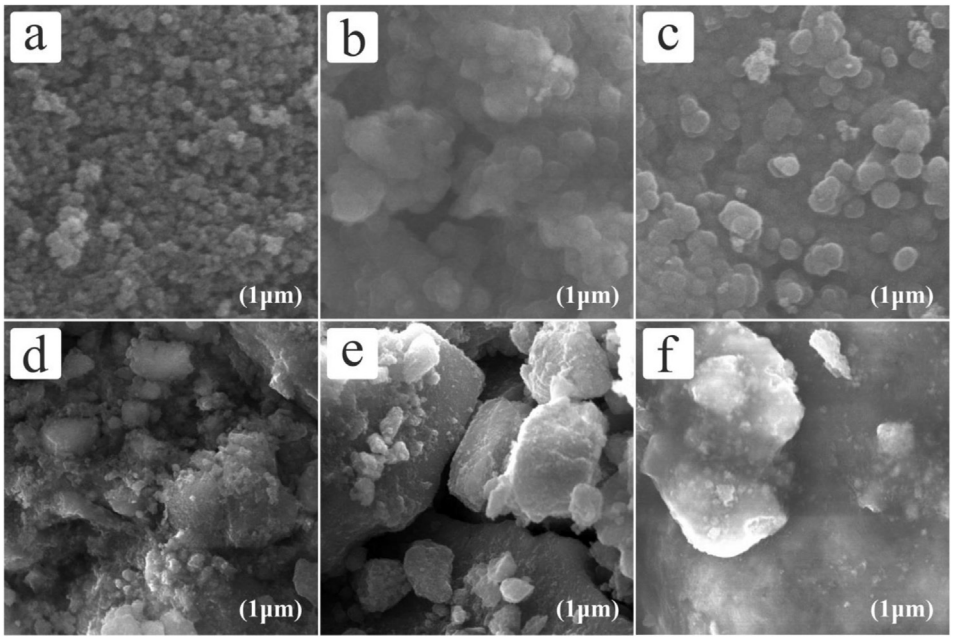

Figure 5. SEM images of a) MNPs, b) Fe_3O_4@SiO_2, c) MNPs-G0, d) MNPs-G1, e) MNPs-G1-Mu, f) MNPs-G2-Mu.

second adsorbents are shown, respectively. Peaks in the wavelength range of 1400–1000 cm^{-1} are the peaks of C–C, C–N, C–O bonds. The formation of C=N band owing to imine group as a weak peak appeared at about 1488–1461 cm^{-1} [40,66]. The peaks of the N–H bond are located at 3657-3677 cm^{-1} and the peaks of the C = O bond are located at 1642-1637 cm^{-1} [13,67, 68, 69, 70].

3.1.2. XRD analysis

The crystal structure of the obtained MNPs has been studied by XRD as can be seen in Figure 3. First, XRD data of nanomaterials were gathered and these obtained data were evaluated by comparing with the standard patterns (Reference code: 98-011-1284). The main peaks occurred at 2Θ = 30.4º, 35.5º, 43.5º, 53.7º, 57.5º and 63.0º, which correspond to (220), (311), (400), (422), (511), and (440), respectively (Figure 3a). These characteristic peaks fit perfectly with the reference pattern which demonstrated Fe_3O_4 magnetite nanoparticles in cubic spinal structure [68,71]. Additionally, it was found that coating processes did not change the characteristic XRD pattern [68]. This means that, modification processes did not affect the crystalline structure of MNPs [72].

3.1.3. TEM and SEM analysis

TEM and SEM were used to obtain information about the morphologic properties and the structure of MNPs and modified MNPs. The images of the TEM and SEM of all nanostructured materials were respectively presented in Figure 4 and Figure 5. According to Figure 4a,

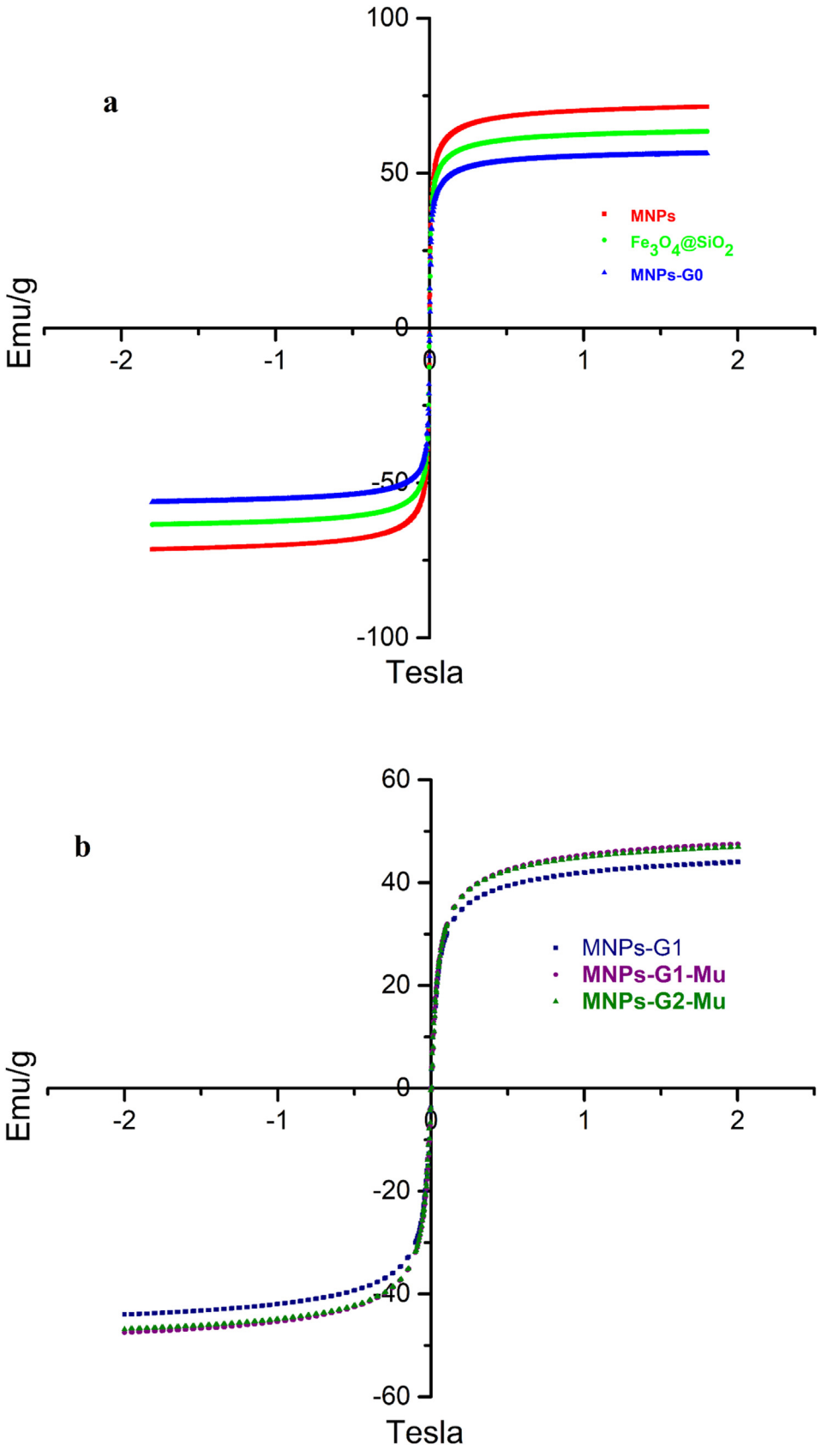

Figure 6. VSM graphics of a) MNPs, $Fe_3O_4@SiO_2$ and MNPS-G0, b) MNPs-G1, MNPs-G1-Mu and MNPs-G2-Mu.

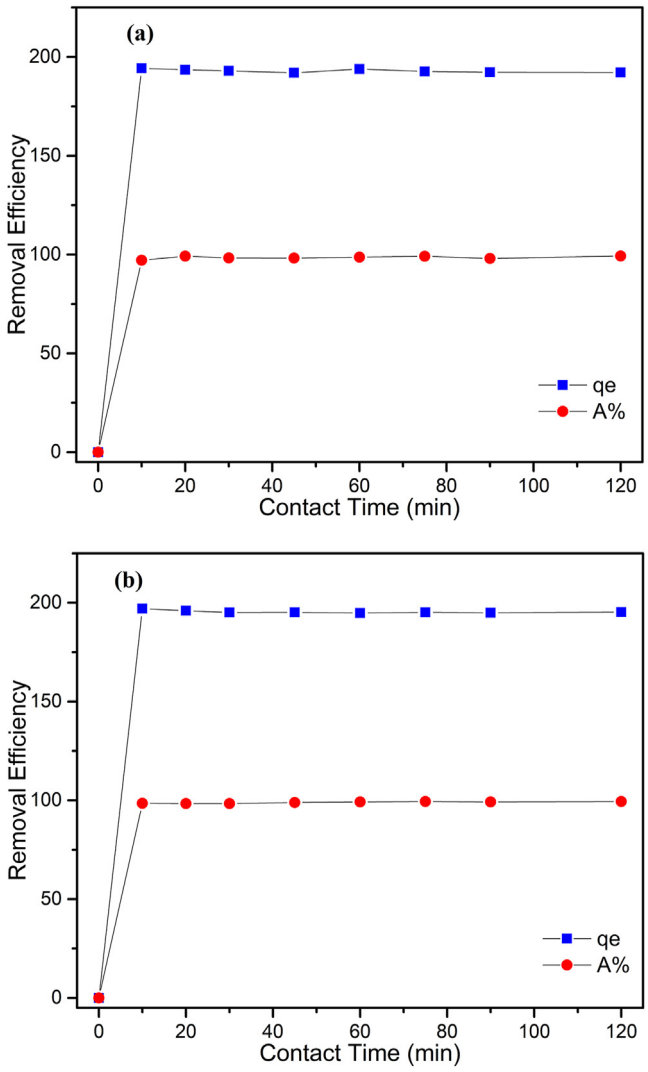

Figure 7. The effect of the contact time on the adsorption of lead (II) by MNPs-G1-Mu (a) and MNPs-G2-Mu (b). (pH = 5, T = 298 K, initial concentration = 100 mg l^{-1} (200 ml), adsorbent amount = 0.05 g, contact time 120 min).

uncoated MNPs look polydisperse and aggregated. MNPs have spherical morphology and core shell mode. Magnetite core appears like black sphere. Particle size of nanoparticles increases with coating processes. The coated layers on the magnetite nanoparticles can be seen in the TEM and SEM images clearly.

3.1.4. VSM analysis

VSM analysis were performed to determine the magnetization properties of MNPs and various organic compounds doped MNPs at room temperature. As can be seen in Figure 6a and 6b, it was determined that the MNPs displayed strong magnetic properties. However, after the particles were coated with silica and APTES, their magnetic properties decreased slightly. At least, the magnetic saturation of MNPs were decreased from 51.6 to 44.5 emu g^{-1} after all coating processes. Although the magnetization saturation value of MNPs decreased after coating, they still continued to exhibit their magnetic properties. As the high saturation magnetization of MNPs-G1-Mu and MNPs-G2-Mu demonstrated, they could be easily taken out from the reaction medium by an external magnetic separator.

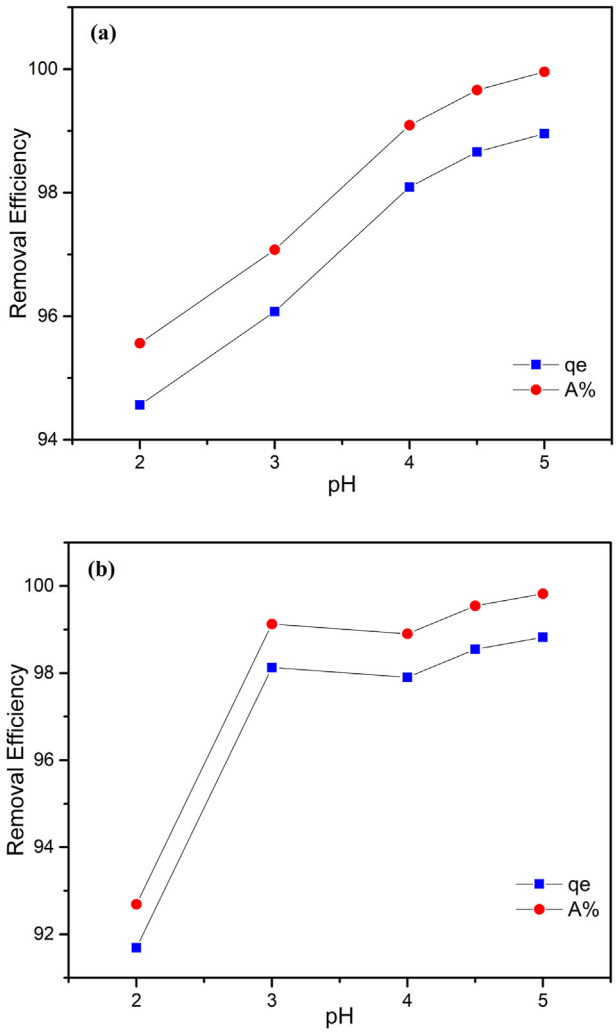

Figure 8. The effect of pH on the adsorption of lead (II) by MNPs-G1-Mu (a) and MNPs-G2-Mu (b). (T = 298 K, initial concentration = 100 mg l^{-1} (50 mL), adsorbent amount = 0.125 g, contact time 30 min).

3.2. The adsorption results

3.2.1. Effects of adsorption parameters

3.2.1.1. Contact time. The effect of contact time on the adsorption of lead (II) ions by MNPs-G1-Mu and MNPs-G2-Mu were investigated in 0–120 min contact time at pH = 5 with 100 mg L^{-1} (200 mL) as initial concentration of lead (II) solution and 50 mg of adsorbents. According to Figure 7a and 7b, adsorption was very fast in the first 10 min because there were electrostatic attraction forces between adsorbents and lead (II). After 10 min, q_e and adsorption percentage values for both adsorption no longer changed. For this reason, optimum contact time was determined as 10 min. The maximum adsorbed lead (II) amounts and adsorption percentage values were 194.24 mg g^{-1} (97.12%) and 196.99 mg g^{-1} (98.49%) for the adsorption of lead (II) by MNPs-G1-Mu and MNPs-G2-Mu, respectively. While the second adsorbent is expected to adsorb more lead (II) ions as it contains more branches, the difference between q_e values of both adsorbent is very small. This situation is probably due to the steric hindrance which occurs with increasing generation of dendrimers.

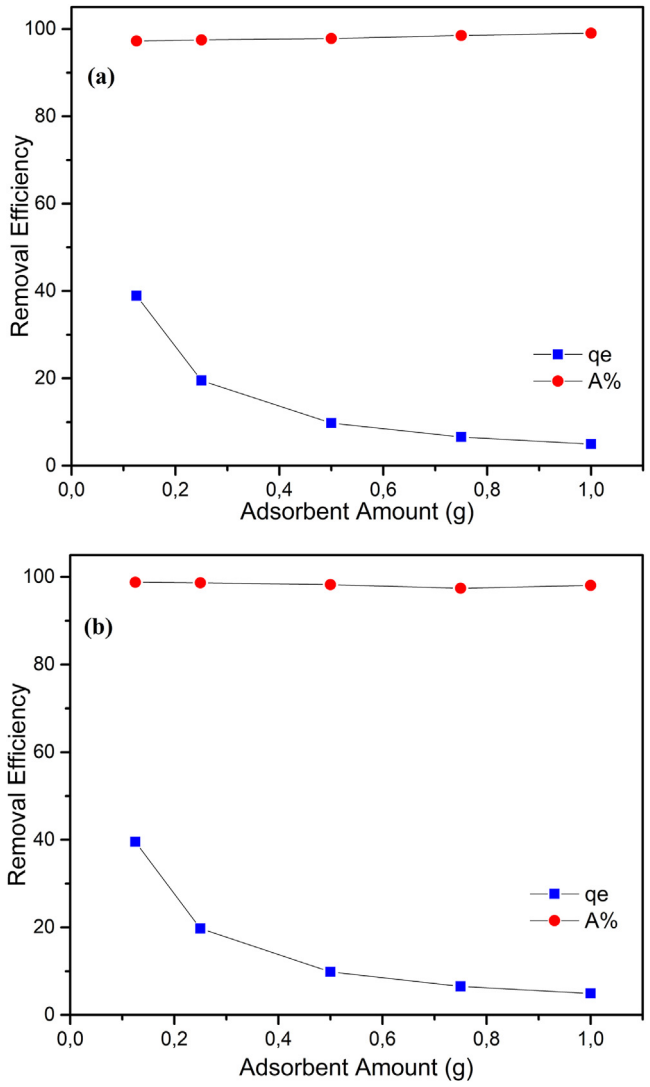

Figure 9. The effect of adsorbent amount on the adsorption of lead (II) by MNPs-G1-Mu (a) and MNPs-G2-Mu (b). (T = 298 K, pH = 5, initial concentration = 100 mg l^{-1} (50 ml), contact time 30 min).

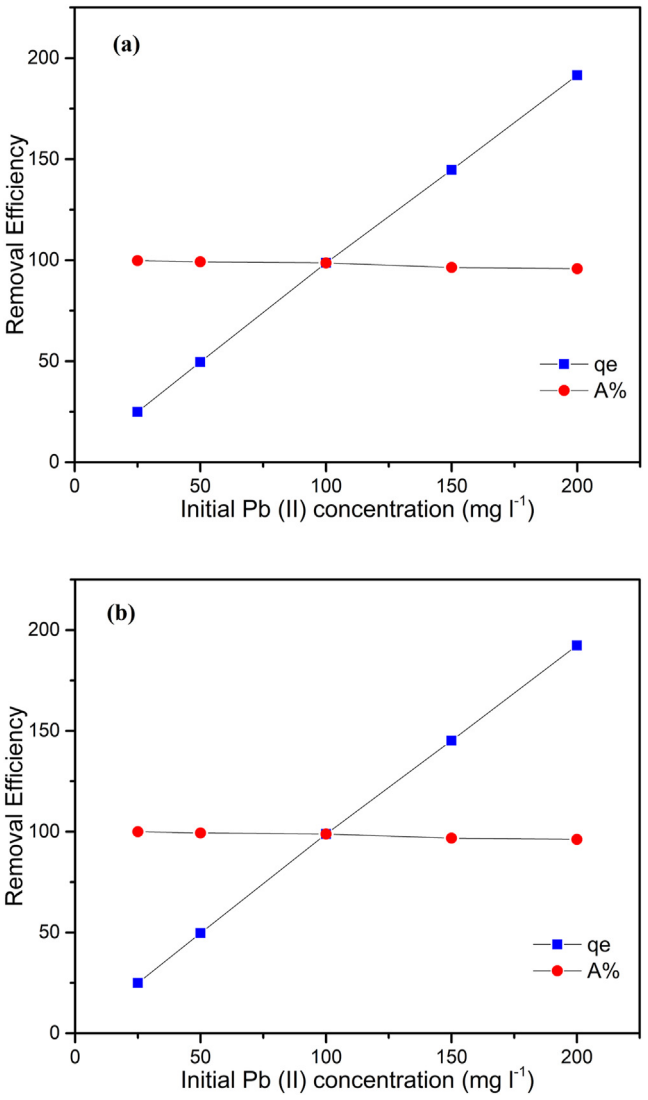

Figure 10. The effect of initial concentration on the adsorption of lead (II) by MNPs-G1-Mu (a) and MNPs-G2-Mu (b). (T = 298 K, pH = 5, adsorbent amount = 0.125 g, contact time 30 min).

3.2.1.2. pH. pH value of the solution is one of the most important parameters for the adsorption processes. The reason is that, pH value of the adsorption media can change due to the dissociation of functional groups of active adsorption areas on the adsorbent surface, surface charge of the adsorbent and ionization degree of materials [49]. Figure 8a and 8b are related to the effect of changing pH value. As seen from these figures, the removal of lead (II) ions from water was affected little by pH of the adsorption media. The maximum adsorption of lead (II) ions on both adsorbents was observed at pH 5. The highest lead (II) ions uptake values obtained for MNPs-G1-Mu and MNPs-G2-Mu were 98.96 mg g^{-1} with adsorption percentage of 99.96 and 98.85 mg g^{-1} with adsorption percentage of 99.82 respectively. The lowest lead (II) uptake values were determined at pH 2 for both adsorbents. (q_e = 94.56 mg g^{-1} and A% = 95.56 for MNPs-G1-Mu and q_e = 91.69 mg g^{-1} and A% = 92.69 for MNPs-G2-Mu at pH 2). Less amount of adsorbed lead (II) ions at low pH values (pH 2) may be due to the fact that the protons found in the solution are more attached to the active adsorption centers of the adsorbents than the metal ions [73]. Both adsorbents adsorbed nearly the same amount of lead (II) ions at pH 5. However, MNPs-G1-Mu adsorbed slightly more lead (II) ions than MNPs-G2-Mu at pH 2. Effect of pH was studied in the pH range of 2–5 because of the precipitation of lead (II) after pH 5 (at pH 6 and higher values of pH) [74].

3.2.1.3. Adsorbent amount. According to the results obtained from Figure 9a and 9b, as the amount of adsorbent increases, the amount of adsorbed lead (II) decreases, but a little change occurs at adsorption percentage which is the same for both absorption processes. One reason for decreasing of the amount of adsorbed lead (II) is the presence of unsaturated adsorption areas; and the other reason is the aggregation of nanoparticles with increasing amount of adsorbent. A similar result is also available in the previous study [75]. q_e values are 38.91 and 39.52 mg g^{-1} for MNPs-G1-Mu and MNPs-G2-Mu, respectively when 0.125 g of adsorbent is used. So, optimum adsorbent amount was selected as 0.125 g for both adsorption process.

3.2.1.4. Initial concentration. The effect of the initial concentration was studied from 25 to 200 mg L^{-1}, and the other parameters were kept constant. As can be observed in Figure 10a and 10b, when initial concentration of lead (II) increases, the adsorbed amount of lead (II) also increases. It is because, when the metal ions concentration is high, there is a possibility that the adsorbents are in contact with a greater amount of metal ions [76]. The percentage of adsorption decreases for both adsorptions with increasing initial concentration. q_e values are 191.57 and 192.30 mg g^{-1} for adsorption of lead (II) at 200 mg L^{-1} concentration by MNPs-G1-Mu and MNPs-G2-Mu, respectively. The adsorption percentage

is the highest at 20 mg L^{-1} initial concentration of lead (II) ions for both adsorbents (99.76% and 99.976%).

3.2.2. Adsorption kinetics

Kinetic studies were applied to find the desired time (without any change in adsorption capacity) which is necessary for the adsorption process to reach equilibrium [77]. Kinetical mechanisms of adsorptions were analyzed by fitting the kinetical data to the pseudo first (Eq. (3)) [78] and second order (Eq. (4)) equations [79]. The linear forms of kinetic equations are given below.

$$\log(q_e - q) = \log q_e - \frac{k_1}{2.303} \cdot t \quad (3)$$

$$\frac{t}{q} = \frac{1}{k_2 q_e^2} + \frac{1}{q_e} t \quad (4)$$

Here; q_e and q (mg g^{-1}) are the adsorbed amount at equilibrium and any time respectively. k_1 (min^{-1}) and k_2 (g mg^{-1} min^{-1}) are first and second order rate constants and t (min) is time. Fitted kinetic curves and related kinetical parameters are shown in Figure 11 and Table 1.

According to R^2 values shown in Table 1, the adsorption of lead (II) on MNPs-G1-Mu is fitted to both pseudo first (R^2 = 0.9705) and second order kinetic equations (R^2 = 0.9908), but R^2 value of pseudo second order equation is higher. It means, the adsorption of lead (II) ions by MNPs-G1-Mu occurs by both physical and chemical sorption. The adsorption of lead (II) on MNPs-G2-Mu is fitted merely to pseudo second order kinetic equation confirmed by 0.9424 value of R^2. Finally, it can be concluded that the adsorption of lead (II) ions by MNPs-G2-Mu takes place through the chemisorption process.

3.2.3. Models of isotherms

Adsorption properties and adsorbent capacity are generally defined by adsorption isotherms. Langmuir and Freundlich linear adsorption isotherms were drawn so as to analyze the adsorption process better. The following equations are Langmuir (5) [80] and Freundlich (6) [81] isotherm equations:

$$\frac{C_e}{q_e} = \frac{1}{q_m b} + \frac{C_e}{q_m} \quad (5)$$

$$\log q_e = \log k + \frac{1}{n} \log C_e \quad (6)$$

here;

q_m (mg g^{-1}), k: Langmuir and Freundlich constants related with maximum adsorption capacity.

b (mg L^{-1}): Langmuir constant related with adsorption energy.

n: Freundlich constant related with adsorption intensity.

Langmuir and Freundlich isotherm constants were calculated from their linear isotherms.

Dimensionless R_L (Eq. (7)) is a specific Langmuir factor indicating the type of the adsorption;

$$R_L = \frac{1}{1 + b.C0} \quad (7)$$

According to R^2 values (Figure 12), the adsorptions of lead (II) on MNPs-G1-Mu and MNPs-G2-Mu are suitable with both isotherm models, but the adsorption of lead (II) on MNPs-G1-Mu is more appropriate for Freundlich model and the adsorption of lead (II) on MNPs-G2-Mu is also more appropriate for Langmuir model owing to higher R^2 values given in Table 2. Langmuir model describes the monolayer homogenous, and Freundlich model describes multi-layer heterogonous adsorption [58]. It is possible that the adsorption process occurs by forming chelates between the O and N atoms in the structure of the adsorbent and lead (II) ions. As q_m values are greater for the adsorption of lead (II) on MNPs-G2, the adsorption capacity of the MNPs-G2-Mu is higher than the adsorption capacity of the MNPs-G1-Mu. R_L value (Table 2) for the adsorption of lead (II) by MNPs-G1-Mu and MNPs-G2-Mu are calculated as 0.0105 and 0.0039 respectively which show a favorable adsorption ($0 < R_L \leq 1$

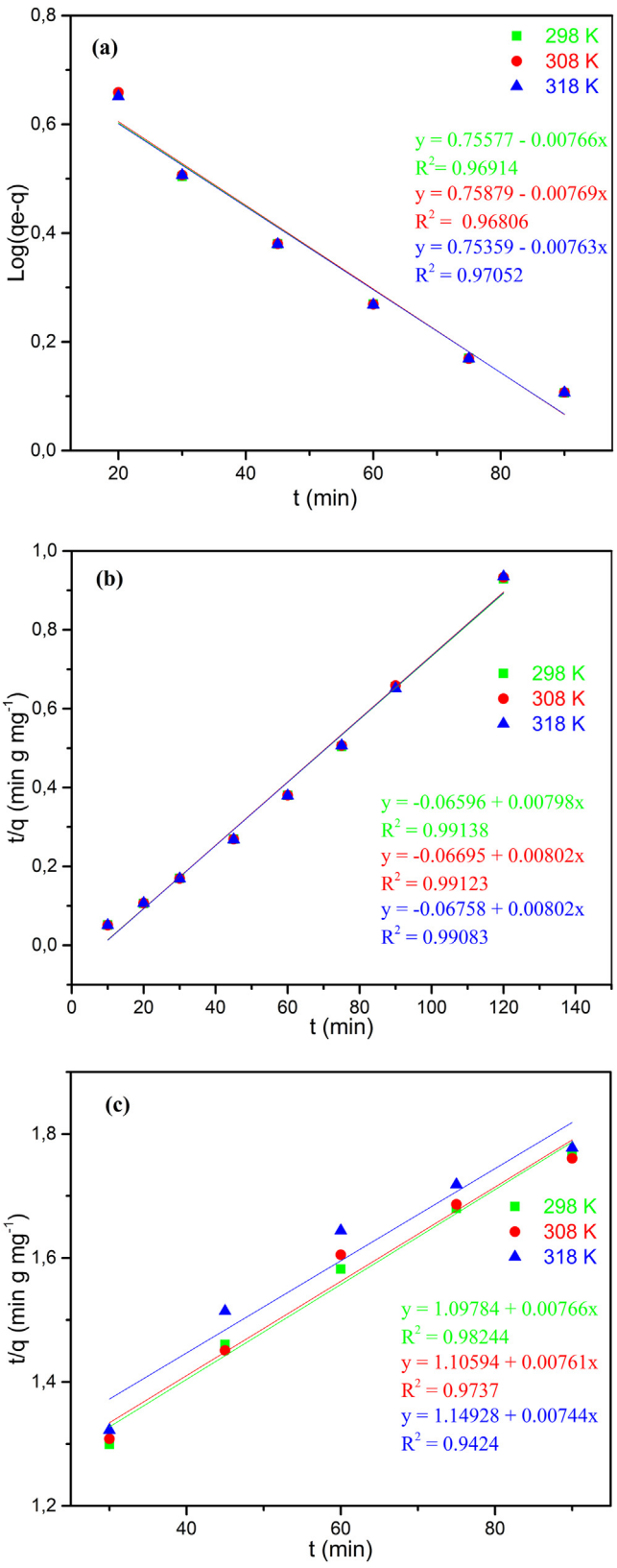

Figure 11. The drawings of Pseudo first order equation for MNPs-G1-Mu (a); and pseudo second order equation for MNPs-G1-Mu (b) and MNPs-G2-Mu (c).

Table 1. Kinetic parameters of adsorptions.

Temperature (°C)	MNPs-G1-Mu				MNPs-G2-Mu			
	Pseudo first order		Pseudo second order		Pseudo first order		Pseudo second order	
	$k_{ads.1}$ (min^{-1})	R^2	$k_{ads.2}$ (g mg^{-1} min^{-1})	R^2	$k_{ads.1}$ (min^{-1})	R^2	$k_{ads.2}$ (g $mg^{-1}min^{-1}$)	R^2
298 K	0.0177	0.9705	0.0082	0.9908	-	-	0.0064	0.9424
308 K	0.0177	0.9681	0.0075	0.9912	-	-	0.0069	0.9737
318 K	0.0175	0.9691	0.0071	0.9914	-	-	0.0070	0.9824

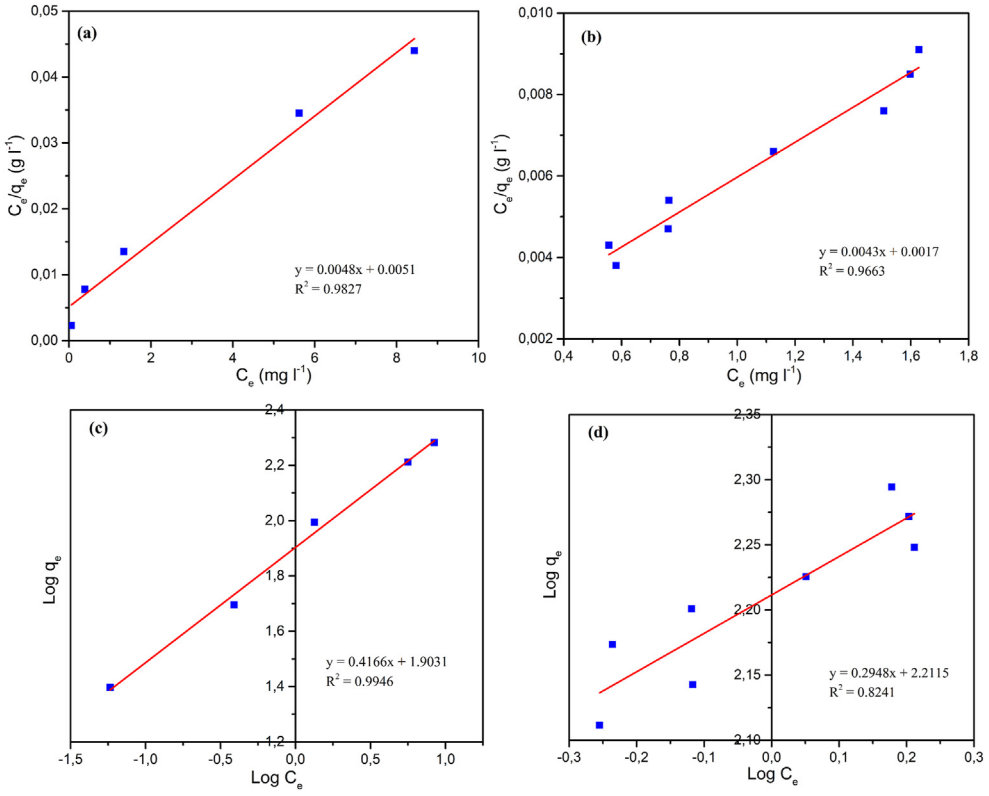

Figure 12. The Langmuir lineer isotherms of the adsorption of lead (II) on MNPs-G1-Mu (a) and MNPs-G2-Mu (b); and the Freundlich lineer isotherms of the adsorption of lead (II) on MNPs-G1-Mu (c) and MNPs-G2-Mu (d). (T = 298 K).

Table 2. Parameters of Langmuir and Freundlich isotherm models.

Adsorbents	Langmuir Constants				Freundlich Constants		
	q_m (mg g^{-1})	b (L mg^{-1})	R_L	R^2	k	n	R^2
MNPs-G1-Mu	208.33	0.9410	0.0105	0.9827	80.0018	2.4	0.9946
MNPs-G2-Mu	232.56	2.5294	0.0039	0.9663	162.742	3.39	0.8241

Table 3. Comparison of adsorption performances of various adsorbents for lead (II).

Adsorbents	Q_{max} (mg g^{-1})	References
MNPs-G1-Mu	208.33	This work
MNPs-G2-Mu	232.56	This work
g-C_3N_4	22.30	Wan et al., 2019 [77]
The original HC	32.67	Jiang et al., 2019 [2]
Fig sawdust activated carbon	80.65	Ghasemi et al., 2014 [78]
M-Lignin-PEI	96.66	Zhang et al., 2019 [10]
Chitosan-beads	72.89	Gyanannath et al., 2012 [79]
Cashew nut shells	28.90	Tangjuank et al., 2009 [80]
Pine cones	27.53	Momčilović et al., 2011 [81]

Figure 13. The FT-IR spectra of MNPs-G1-Mu after adsorption.

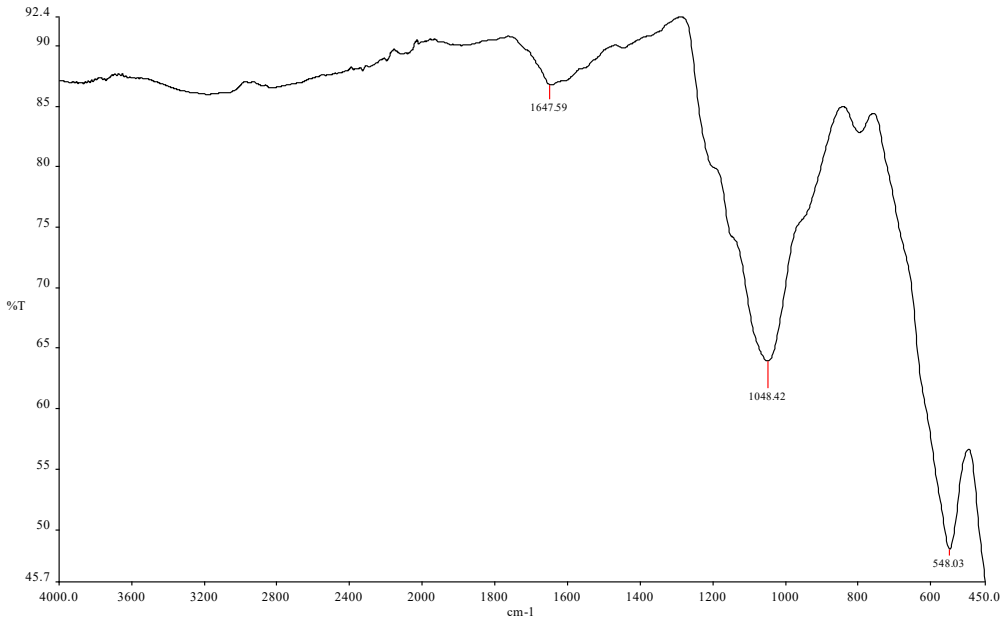

Figure 14. The FT-IR spectra of MNPs-G2-Mu after adsorption.

provide favorable adsorption conditions). Finally, in these adsorption processes, a combination of Langmuir and Freundlich isotherm model was observed.

3.2.4. Comparison of maximum adsorption capacities of different adsorbents

The maximum adsorption capacities (q_m) were calculated by the Langmuir equation for lead (II) on MNPs-G1-Mu and on MNPs-G2-Mu as 208.33 and 232.56 mg g^{-1}, respectively. The calculated q_m values proved that synthesized adsorbents had high adsorption capacities. In this study, great results were obtained due to strong interaction that happened between lead (II) ions and nitrogen atoms. q_m values for lead (II) reported for other adsorbents are shown in Table 3. Generally, utilized nanostructured adsorbents had higher adsorption capacity than the other reported adsorbents at Table 3 [2,10,82, 83, 84, 85, 86]. Moreover,

Table 4. Results of antimicrobial activity of nanoparticles against some microorganisms.

	P. aeruginosa ATCC 27853	*E. coli ATTC 25922*	*K. pneumoniae ATCC 4352*	*P. mirabilis ATCC14153*	*E. faecalis ATCC 29212*	*S. epidermidis ATCC 12228*	*S. aureus ATCC 29213*	*C. albicans ATCC 10231*	*C. parapsilosis ATCC 22019*
MNPs-G1-Mu	-	-	-	-	-	-	625	312.5	78.12
MNPs-G2-Mu	-	-	-	-	-	-	625	-	625
Pb^{+2} adsorbed MNPs-G2-Mu	-	-	-	-	-	-	625	-	625
Fe_3O_4 Control	-	-	-	-	-	-	-	-	625

considering their easy preparation and separation, MNPs-G1-Mu and MNPs-G2-Mu are better adsorbents compared to the others.

The FT-IR spectras of adsorbents exposed to lead (II) ions are shown in Figures 13 and 14.

The FT-IR spectras of adsorbents exposed to lead (II) ions are slightly lower than the non-metal loaded FT-IR spectrum. Some peaks previously seen in the FT-IR spectrum of adsorbents are no longer visible. After adding lead (II), Pb–N and Pb–O interactions are shown at around 1640 and 1040 cm^{-1} (Figures 13 and 14) [74]. So, these spectras are also prove that the adsorption process occurs by forming chelates between the O and N atoms in the structure of the adsorbent and lead (II) ions.

3.3. The results of antimicrobial activity

The results in Table 4 indicate that; at least 625 (μg mL^{-1}) of MNPs-G1-Mu, MNPs-G2-Mu and lead (II) adsorbed MNPs-G2-Mu are required to prevent the growth of S. aureus ATTC 29213. The lowest concentration of MNPs-G1-Mu should be 312.5 (μg mL^{-1}) to prevent the growth of the C. albican ATTC 10231. The lowest concentration of MNPs-G2-Mu, lead (II) adsorbed MNPs-G2-Mu and Fe_3O_4 (control) should be 625 (μg mL^{-1}) to prevent the growth of the C. parapsilosis ATTC 22019. The lowest concentration of MNPs-G1-Mu should be 78.12 (μg mL^{-1}) to prevent the growth of the C. parapsilosis ATTC 22019. As a result, MNPs-G1-Mu showed the most antimicrobial activity against C. parapsilosis ATTC 22019. MNPs-G2-Mu and lead (II) adsorbed MNPs-G2-Mu showed antimicrobial activity against both C. parapsilosis ATTC 22019 and S. aureus ATTC 29213. Only MNPs-G1-Mu showed antimicrobial activity against C. albican ATTC 10231. Synthesized nanoparticles didn't show antimicrobial activity against the other microorganisms. Fe_3O_4 nanoparticles (control) showed antimicrobial activity against only C. parapsilosis ATCC 22019. However, MNPs-G1-Mu, MNPs-G2-Mu and lead (II) adsorbed MNPs-G2-Mu exhibited antimicrobial activity against two other microorganisms besides C. parapsilosis ATCC 22019. So, it indicates that; the coating of iron oxide nanoparticles enhanced the antimicrobial activity of them.

4. Conclusions

In this study, new nano-sized, magnetite-cored and environmentally friendly MNPs encapsulated with Mu-terminated PAMAM for uptaking of lead (II) from aqueous environment were successfully prepared. The obtained nanomaterials were characterized by different spectroscopic techniques. The ability of the magnetite nanostructured adsorbents for taking out lead (II) from diluted solution by using batch method were explored. And also antimicrobial activities of nanomaterials against various microorganisms were tested. Adsorption processes with both adsorbents were highly fast and effective and adsorbents were easily recollected after adsorption processes due to their magnetic properties. High q_m values of adsorbents were 208.33 and 232.56 mg g^{-1} for MNPs-G1-Mu and MNPs-G2-Mu, respectively. The adsorption parameters influenced both adsorption processes almost equally. Owing to the fact that q_m value of MNPs-G2-Mu is higher than MNPs-G1-Mu, it is expected to be slightly more effective for uptaking lead (II) ions. However, the adsorption results were close to each other. It is probable that this situation stems from the steric hindrance which occurs with increasing generation of dendrimers. Adsorption parameters for both adsorptions were determined as pH = 5, 0.125 g adsorbent amount, lead (II) concentration of 200 mg L^{-1} during 10 min contact time. The adsorption process occurs by forming the electrostatic attraction forces between the O and N atoms in the structure of the adsorbents and lead (II) ions. Adsorption kinetics of MNPs-G1-Mu were fitted by only pseudo first order model, however adsorption kinetics of MNPs-G2-Mu were fitted by both pseudo first and second order model. Adsorption processes made with both adsorbents were also compatible with both Langmuir and Freundlich adsorption isotherms. However, according to R^2 values adsorption by MNPs-G1-Mu indicated more compatibility with Freundlich isotherm; and adsorption by MNPs-G2-Mu exhibited more compatibility with Langmuir isotherm. As a result of this study, it was determined that our results, which were better than the other results reported, exhibited high binding affinity for removal of lead (II) from aqueous media. Antimicrobial activities of MNPs-G1-Mu, and MNPs-G2-Mu, MNPs and lead (II) adsorbed onto MNPs-G2-Mu against nine different species were examined. MNPs-G1-Mu displayed antimicrobial activities against C. albicans and *C. Parapsilosis*. Synthesized nanomaterials can be suggested as adsorbents for adsorption of lead (II) and antimicrobial agents against C. albicans and *C. Parapsilosis*.

Finally, we can say that the removal of lead (II) from aqueous solutions with the magnetic separation method using the nanoadsorbents is a relatively easy and cost effective procedure compared to other alternative methods.

Declarations

Author contribution statement

Selma Ekinci: Conceived and designed the experiments; Performed the experiments; Analyzed and interpreted the data; Wrote the paper.

Zülfiye İlter, Ercan Çınar: Analyzed and interpreted the data; Contributed reagents, materials, analysis tools or data.

Selami Ercan: Analyzed and interpreted the data; Wrote the paper.

Reşit Çakmak: Conceived and designed the experiments; Wrote the paper.

Funding statement

The study is supported by Firat University Scientific Research Projects Management Unit (FF.1638).

Data availability statement

Data included in article/supplementary material/referenced in article.

Declaration of interests statement

The authors declare no conflict of interest.

Additional information

No additional information is available for this paper.

References

[1] A. Begum, M. Ramaiah, I. Khan, K. Veena, Heavy metal pollution and chemical profile of Cauvery River water, J. Chem. 6 (2009) 47–52.

[2] Q. Jiang, W. Xie, S. Han, Y. Wang, Y. Zhang, Enhanced adsorption of Pb (II) onto modified hydrochar by polyethyleneimine or H_3PO_4: an analysis of surface property and interface mechanism, Colloid. Surface. 583 (2019) 123962.

[3] Y. Li, Q. Zhou, B. Ren, J. Luo, J. Yuan, X. Ding, H. Bian, X. Yao, Trends and health risks of dissolved heavy metal pollution in global river and lake water from 1970 to 2017, Rev. Environ. Contam. Toxicol. 251 (2019) 1–24.

[4] M. Rashed, Monitoring of environmental heavy metals in fish from Nasser Lake, Environ. Int. 27 (2001) 27–33.

[5] S. Zhao, H. Zhu, H. Wang, P. Rassu, Z. Wang, P. Song, D. Rao, Free-standing graphene oxide membrane with tunable channels for efficient water pollution control, J. Hazard Mater. 366 (2019) 659–668.

[6] F. Aydin, R. Çakmak, A. Levent, M. Soylak, Silica Gel-Immobilized 5-aminoisophthalohydrazide: a novel sorbent for solid phase extraction of Cu, Zn and Pb from natural water samples, Appl. Organomet. Chem. (2020), e5481.

[7] D.B. Barr, R.Y. Wang, L.L. Needham, Biologic monitoring of exposure to environmental chemicals throughout the life stages: requirements and issues for consideration for the National Children's Study, Environ. Health Perspect. 113 (2005) 1083–1091.

[8] C. Filote, I. Volf, S.C. Santos, C.M. Botelho, Bioadsorptive removal of Pb (II) from aqueous solution by the biorefinery waste of Fucus spiralis, Sci. Total Environ. 648 (2019) 1201–1209.

[9] C. Martınez, H. Motto, Solubility of lead, zinc and copper added to mineral soils, Environ. Pollut. 107 (2000) 153–158.

[10] X. Zhang, Y. Li, Y. Hou, Preparation of magnetic polyethylenimine lignin and its adsorption of Pb (II), Int. J. Biol. Macromol. 141 (2019) 1102–1110.
[11] B. Dong, R. Zhang, Y. Gan, L. Cai, A. Freidenreich, K. Wang, T. Guo, H. Wang, Multiple methods for the identification of heavy metal sources in cropland soils from a resource-based region, Sci. Total Environ. 651 (2019) 3127–3138.
[12] S. Dhiman, B. Gupta, Partition studies on cobalt and recycling of valuable metals from waste Li-ion batteries via solvent extraction and chemical precipitation, J. Clean. Prod. 225 (2019) 820–832.
[13] F. Ge, M.-M. Li, H. Ye, B.-X. Zhao, Effective removal of heavy metal ions Cd^{2+}, Zn^{2+}, Pb^{2+}, Cu^{2+} from aqueous solution by polymer-modified magnetic nanoparticles, J. Hazard Mater. 211 (2012) 366–372.
[14] I.B. Rae, S. Pap, D. Svobodova, S.W. Gibb, Comparison of sustainable biosorbents and ion-exchange resins to remove Sr^{2+} from simulant nuclear wastewater: batch, dynamic and mechanism studies, Sci. Total Environ. 650 (2019) 2411–2422.
[15] M. Ruthiraan, N. Mubarak, E. Abdullah, M. Khalid, S. Nizamuddin, R. Walvekar, R.R. Karri, An Overview of Magnetic Material: Preparation and Adsorptionremoval of Heavy Metals from Wastewater, Magnetic Nanostructures, Springer, 2019, pp. 131–159.
[16] Y.-J. Shih, S.-K. Chien, S.-R. Jhang, Y.-C. Lin, Chemical leaching, precipitation and solvent extraction for sequential separation of valuable metals in cathode material of spent lithium ion batteries, J. Taiwan Inst. Chem. E 100 (2019) 151–159.
[17] B.S. Thaçi, S.T. Gashi, Reverse osmosis removal of heavy metals from wastewater effluents using biowaste materials pretreatment, Pol. J. Environ. Stud. 28 (2019).
[18] K. Yin, Q. Wang, M. Lv, L. Chen, Microorganism remediation strategies towards heavy metals, Chem. Eng. J. 360 (2019) 1553–1563.
[19] N.N. Nassar, Kinetics, equilibrium and thermodynamic studies on the adsorptive removal of nickel, cadmium and cobalt from wastewater by superparamagnetic iron oxide nanoadsorbents, Can. J. Chem. Eng. 90 (2012) 1231–1238.
[20] Y. Shen, J. Tang, Z. Nie, Y. Wang, Y. Ren, L. Zuo, Preparation and application of magnetic Fe_3O_4 nanoparticles for wastewater purification, Separ. Purif. Technol. 68 (2009) 312–319.
[21] P.G. Tratnyek, R.L. Johnson, Nanotechnologies for environmental cleanup, Nano. Today 1 (2006) 44–48.
[22] J.-H. Lin, Z.-H. Wu, W.-L. Tseng, Extraction of environmental pollutants using magnetic nanomaterials, Anal. Meth. 2 (2010) 1874–1879.
[23] N. Parham, H.A. Panahi, A. Feizbakhsh, E. Moniri, Synthesis of high generation thermo-sensitive dendrimers for extraction of rivaroxaban from human fluid and pharmaceutic samples, J. Chromatogr. A 1545 (2018) 12–21.
[24] L. Sun, C. Zhang, L. Chen, J. Liu, H. Jin, H. Xu, L. Ding, Preparation of alumina-coated magnetite nanoparticle for extraction of trimethoprim from environmental water samples based on mixed hemimicelles solid-phase extraction, Anal. Chim. Acta 638 (2009) 162–168.
[25] X. Zhang, H. Niu, Y. Pan, Y. Shi, Y. Cai, Chitosan-coated octadecyl-functionalized magnetite nanoparticles: preparation and application in extraction of trace pollutants from environmental water samples, J. Anal. Chem. 82 (2010) 2363–2371.
[26] A. Maleki, Fe_3O_4/SiO_2 nanoparticles: an efficient and magnetically recoverable nanocatalyst for the one-pot multicomponent synthesis of diazepines, Tetrahedron 68 (2012) 7827–7833.
[27] G.H. Mirzabe, A.R. Keshtkar, Application of response surface methodology for thorium adsorption on PVA/Fe_3O_4/SiO_2/APTES nanohybrid adsorbent, J. Ind. Eng. Chem. 26 (2015) 277–285.
[28] E.B. Bahadır, M.K. Sezgintürk, Poly (amidoamine)(PAMAM): an emerging material for electrochemical bio (sensing) applications, Talanta 148 (2016) 427–438.
[29] N. Bono, C. Pennetta, M.C. Bellucci, A. Sganappa, C. Malloggi, G. Tedeschi, G. Candiani, A. Volonterio, Role of generation on successful DNA delivery of PAMAM–(guanidino) neomycin conjugates, ACS Omega 4 (2019) 6796–6807.
[30] M.K. Calabretta, A. Kumar, A.M. McDermott, C. Cai, Antibacterial activities of poly (amidoamine) dendrimers terminated with amino and poly (ethylene glycol) groups, Biomacromolecules 8 (2007) 1807–1811.
[31] B. Klaykruayat, K. Siralertmukul, K. Srikulkit, Chemical modification of chitosan with cationic hyperbranched dendritic polyamidoamine and its antimicrobial activity on cotton fabric, Carbohydr. Polym. 80 (2010) 197–207.
[32] P.K. Maiti, T. Çağın, G. Wang, W.A.J.M. Goddard, Structure of PAMAM dendrimers: Generations 1 through 11, Macromol. 11 (37) (2004) 6236–6254.
[33] B. Maleki, M. Baghayeri, M. Ghanei-Motlagh, F.M. Zonoz, A. Amiri, F. Hajizadeh, A. Hosseinifar, E.J.M. Esmaeilnezhad, Polyamidoamine dendrimer functionalized iron oxide nanoparticles for simultaneous electrochemical detection of Pb2+ and Cd2+ ions in environmental waters, Measure. 140 (2019) 81–88.
[34] D.A. Tomalia, H. Baker, J. Dewald, M. Hall, G. Kallos, S. Martin, J. Roeck, J. Ryder, P.J.M. Smith, Dendritic macromolecules, Synth. Starburst Dendri. 19 (1986) 2466–2468.
[35] R. Esfand, D.A.J. Tomalia, Poly (amidoamine)(PAMAM) dendrimers: from biomimicry to drug delivery and biomedical applications, Drug Discov. Today 6 (2001) 427–436.
[36] T. Fu, Y. Niu, Y. Zhou, K. Wang, Q. Mu, R. Qu, H. Chen, B. Yuan, H. Yang, Adsorption of Mn (II) from aqueous solution by silica-gel supported polyamidoamine dendrimers: experimental and DFT study, J. Taiwan Inst. Chem. E 97 (2019) 189–199.
[37] Y. Niu, R. Qu, C. Sun, C. Wang, H. Chen, C. Ji, Y. Zhang, X. Shao, F. Bu, Adsorption of Pb (II) from aqueous solution by silica-gel supported hyperbranched polyamidoamine dendrimers, J. Hazard Mater. 244 (2013) 276–286.
[38] X. Wu, L. Luo, Z. Chen, K. Liang, Syntheses, characterization and adsorption properties for Pb^{2+} of silica-gel functionalized by dendrimer-like polyamidoamine and 5-sulfosalicylic acid, Appl. Surf. Sci. 364 (2016) 86–95.
[39] E. Guibal, Interactions of metal ions with chitosan-based sorbents: a review, Separ. Purif. Technol. 38 (2004) 43–74.
[40] R. Li, Q. He, Z. Hu, S. Zhang, L. Zhang, X. Chang, Highly selective solid-phase extraction of trace Pd (II) by murexide functionalized halloysite nanotubes, Anal. Chim. Acta 713 (2012) 136–144.
[41] X. Li, X. Wang, D. Chen, S. Chen, Antioxidant activity and mechanism of protocatechuic acid in vitro, Funct. Food Health Dis. 1 (2011) 232–244.
[42] S. Sadeghi, E. Sheikhzadeh, Solid phase extraction using silica gel modified with murexide for preconcentration of uranium (VI) ions from water samples, J. Hazard Mater. 163 (2009) 861–868.
[43] H. Schatzmann, Dependence on calcium concentration and stoichiometry of the calcium pump in human red cells, J. Physiol. 235 (1973) 551–569.
[44] M. Cheira, M. Rashed, A. Mohamed, G. Hussein, M. Awadallah, Removal of some harmful metal ions from wet-process phosphoric acid using murexide-reinforced activated bentonite, Mater. Today Chem. 14 (2019) 100176.
[45] A. Maleki, R. Rahimi, S. Maleki, N. Hamidi, Synthesis and characterization of magnetic bromochromate hybrid nanomaterials with triphenylphosphine surface-modified iron oxide nanoparticles and their catalytic application in multicomponent reactions, RSC Adv. 4 (2014) 29765–29771.
[46] R. Rahimi, A. Maleki, S. Maleki, A. Morsali, M.J. Rahimi, Synthesis and characterization of magnetic dichromate hybrid nanomaterials with triphenylphosphine surface modified iron oxide nanoparticles (Fe_3O_4@SiO_2@PPh_3@$Cr_2O_7^{2-}$), Solid State Sci. 28 (2014) 9–13.
[47] R. Çakmak, G. Topal, E. Çınar, Covalent immobilization of Candida rugosa lipase on epichlorohydrin-coated magnetite nanoparticles: enantioselective hydrolysis studies of some racemic esters and HPLC analysis, Appl. Biochem. Biotechnol. (2020) 1–21.
[48] D. Maity, D. Agrawal, Synthesis of iron oxide nanoparticles under oxidizing environment and their stabilization in aqueous and non-aqueous media, J. Magn. Magn Mater. 308 (2007) 46–55.
[49] T. Wang, W.-L. Yang, Y. Hong, Y.-L. Hou, Magnetic nanoparticles grafted with amino-riched dendrimer as magnetic flocculant for efficient harvesting of oleaginous microalgae, Chem. Eng. J. 297 (2016) 304–314.
[50] A. Gholami, S. Rasoul-Amini, A. Ebrahiminezhad, N. Abootalebi, U. Niroumand, N. Ebrahimi, Y. Ghasemi, Magnetic properties and antimicrobial effect of amino and lipoamino acid coated iron oxide nanoparticles, Minerva Biotecnol. 28 (2016) 177–186.
[51] N. Ildiz, A. Baldemir, C. Altinkaynak, N. Özdemir, V. Yilmaz, I. Ocsoy, Self assembled snowball-like hybrid nanostructures comprising Viburnum opulus L. extract and metal ions for antimicrobial and catalytic applications, Enzym. Microb. Technol. 102 (2017) 60–66.
[52] M. Mukherje, In vitro antimicrobial activity of polyacrylamide doped magnetic iron oxide nanoparticles, Int. J. Mech. Mater. Des. 2 (2014) 64–66.
[53] D.P. Tamboli, D.S. Lee, Mechanistic antimicrobial approach of extracellularly synthesized silver nanoparticles against gram positive and gram negative bacteria, J. Hazard Mater. 260 (2013) 878–884.
[54] M. Khalkhali, S. Sadighian, K. Rostamizadeh, F. Khoeini, M. Naghibi, N. Bayat, M. Habibizadeh, M. Hamidi, Synthesis and characterization of dextran coated magnetite nanoparticles for diagnostics and therapy, Bioimpacts 5 (2015) 141–150.
[55] M. Ma, Y. Zhang, W. Yu, H.-y. Shen, H.-q. Zhang, N. Gu, Preparation and characterization of magnetite nanoparticles coated by amino silane, Colloids Surf. A 212 (2003) 219–226.
[56] B.-f. Pan, F. Gao, H.-C. Gu, Dendrimer modified magnetite nanoparticles for protein immobilization, J. Colloid Interface Sci. 284 (2005) 1–6.
[57] L. White, C. Tripp, Reaction of (3-aminopropyl) dimethylethoxysilane with amine catalysts on silica surfaces, J. Colloid Interface Sci. 232 (2000) 400–407.
[58] S. Aliannejadi, A.H. Hassani, H.A. Panahi, S.M. Borghei, Fabrication and characterization of high-branched recyclable PAMAM dendrimer polymers on the modified magnetic nanoparticles for removing naphthalene from aqueous solutions, Microchem. J. 145 (2019) 767–777.
[59] B. Saif, C. Wang, D. Chuan, S. Shuang, Synthesis and characterization of Fe_3O_4 coated on APTES as carriers for morin-anticancer drug, J. Biomat. Nanobiotech. 6 (2015) 267–275.
[60] Y. Wang, P. Su, S. Wang, J. Wu, J. Huang, Yang, Dendrimer modified magnetic nanoparticles for immobilized BSA: a novel chiral magnetic nano-selector for direct separation of racemates, J. Mater. Chem. B 1 (2013) 5028–5035.
[61] P.A. Heiney, K. Grüneberg, J. Fang, C. Dulcey, R. Shashidhar, Structure and growth of chromophore-functionalized (3-aminopropyl) triethoxysilane self-assembled on silicon, Langmuir 16 (2000) 2651–2657.
[62] N. Kemikli, H. Kavas, S. Kazan, A. Baykal, R. Ozturk, Synthesis of protoporphyrin coated superparamagnetic iron oxide nanoparticles via dopamine anchor, J. Alloys Compd. 502 (2010) 439–444.
[63] P. Launer, B.J.G. Arkles, Inc, Silicon Compounds, Silanes and Silicones, 2013, pp. 175–178.
[64] Y. Jiang, J. Jiang, Q. Gao, M. Ruan, H. Yu, L. Qi, A novel nanoscale catalyst system composed of nanosized Pd catalysts immobilized on Fe_3O_4@SiO_2–PAMAM, Nanotech. 19 (2008), 075714.
[65] M. Tajabadi, M.E. Khosroshahi, S. Bonakdar, An efficient method of SPION synthesis coated with third generation PAMAM dendrimer, Colloids Surf. A Physicochem. Eng. Asp. 431 (2013) 18–26.

[66] A. Pereira, G. Ferreira, L. Caetano, M. Martines, P. Padilha, A. Santos, G. Castro, Preconcentration and determination of Cu (II) in a fresh water sample using modified silica gel as a solid-phase extraction adsorbent, J. Hazard Mater. 175 (2010) 399–403.
[67] J.-J. Jung, J.-W. Jang, J.-W. Park, Effect of generation growth on photocatalytic activity of nano TiO_2-magnetic cored dendrimers, J. Ind. Eng. Chem. 44 (2016) 52–59.
[68] R. Khodadust, G. Unsoy, S. Yalcın, G. Gunduz, U. Gunduz, PAMAM dendrimer-coated iron oxide nanoparticles: synthesis and characterization of different generations, J. Nanoparticle Res. 15 (2013) 1488.
[69] T. Tarhan, B. Tural, S. Tural, G. Topal, Enantioseparation of mandelic acid enantiomers with magnetic nano-sorbent modified by a chiral selector, Chirality 27 (2015) 835–842.
[70] W. Wu, Q. He, C. Jiang, Magnetic iron oxide nanoparticles: synthesis and surface functionalization strategies, Nanoscale Res. Lett. 3 (2008) 397.
[71] U. Kurtan, A. Baykal, Fabrication and characterization of Fe_3O_4@ APTES@ PAMAM-Ag highly active and recyclable magnetic nanocatalyst: catalytic reduction of 4-nitrophenol, Mater. Res. Bull. 60 (2014) 79–87.
[72] N. Arsalani, H. Fattahi, M. Nazarpoor, Synthesis and characterization of PVP-functionalized superparamagnetic Fe_3O_4 nanoparticles as an MRI contrast agent, Express Polym. Lett. 4 (2010) 329–338.
[73] M. Basu, A.K. Guha, L. Ray, Adsorption of lead on cucumber peel, J. Clean. Prod. 151 (2017) 603–615.
[74] Z. Baysal, E. Cinar, Y. Bulut, H. Alkan, M. Dogru, Equilibrium and thermodynamic studies on biosorption of Pb (II) onto Candida albicans biomass, J. Hazard Mater. 161 (2009) 62–67.
[75] K. Padmavathy, G. Madhu, P. Haseena, A study on effects of pH, adsorbent dosage, time, initial concentration and adsorption isotherm study for the removal of hexavalent chromium (Cr (VI)) from wastewater by magnetite nanoparticles, Proc. Technol. 24 (2016) 585–594.
[76] S.V. Mousavi, A. Bozorgian, N. Mokhtari, M.A. Gabris, H.R. Nodeh, W.A.W. Ibrahim, A novel cyanopropylsilane-functionalized titanium oxide magnetic nanoparticle for the adsorption of nickel and lead ions from industrial wastewater: equilibrium, kinetic and thermodynamic studies, Microchem. J. 145 (2019) 914–920.
[77] C.B. Vidal, A.L. Barros, C.P. Moura, A.C. De Lima, F.S. Dias, L.C. Vasconcellos, P.B. Fechine, R.F. Nascimento, Adsorption of polycyclic aromatic hydrocarbons from aqueous solutions by modified periodic mesoporous organosilica, J. Colloid Interface Sci. 357 (2011) 466–473.
[78] S. Lagrergen, Zur theorie der sogenannten adsorption gelöster stoffe kunglia svenska Vatenskapsakademiens Handlingar 24 (1898) 1–39.
[79] Y.-S. Ho, G. McKay, Pseudo-second order model for sorption processes, Process Biochem. 34 (1999) 451–465.
[80] I. Langmuir, The adsorption of gases on plane surfaces of glass, mica and platinum, J. Am. Chem. Soc. 40 (1918) 1361–1403.
[81] H. Freundlich, H. Hatfield, Colloid & Capillary Chemistry, Methuen & Company Limited, 1926.
[82] M. Ghasemi, M. Naushad, N. Ghasemi, Y. Khosravi-Fard, A novel agricultural waste based adsorbent for the removal of Pb (II) from aqueous solution: kinetics, equilibrium and thermodynamic studies, J. Ind. Eng. Chem. 20 (2014) 454–461.
[83] G. Gyananath, D. Balhal, Removal of lead (II) from aqueous solutions by adsorption onto chitosan beads, Cellul. Chem. Technol. 46 (2012) 121–124.
[84] M. Momčilović, M. Purenović, A. Bojić, A. Zarubica, M. Ranđelović, Removal of lead (II) ions from aqueous solutions by adsorption onto pine cone activated carbon, Desalination 276 (2011) 53–59.
[85] S. Tangjuank, N. Insuk, J. Tontrakoon, V. Udeye, Adsorption of lead (II) and cadmium (II) ions from aqueous solutions by adsorption on activated carbon prepared from cashew nut shells, Int. Scholar. Sci. Res. Innov. 52 (2009) 110–116.
[86] X. Wan, M.A. Khan, F. Wang, M. Xia, W. Lei, S. Zhu, C. Fu, Y. Ding, Facile synthesis of protonated g-C_3N_4 and acid-activated montmorillonite composite with efficient adsorption capacity for $PO4^{3-}$ and Pb (II), Chem. Eng. Res. Des. 152 (2019) 95–105.